MADRID
inter.noise 2019
June 16 - 19
NOISE CONTROL FOR A BETTER ENVIRONMENT

Frequency and temperature dependent viscoelastic vibration damping capability of a novel local CLD treatment

M. Gröhlich[1], M. Böswald[2], R. Winter[3]
German Aerospace Center (DLR)
Institute of Aeroelasticity
Department for Structural Dynamics and System Identification
Bunsenstraße 10, D-37073 Göttingen, Germany

ABSTRACT

As lightweight and stiffened structures, aircraft are prone to vibration. Constrained Layer Damping (CLD) treatment is a popular method to increase the vibration damping of such structures. Constrained by a top and bottom layer, the viscoelastic core layer is forced under shear strain and causes a dissipation of vibrational energy. However, the damping behaviour of viscoelastic materials is highly dependent on frequency and temperature, and has to be considered during the design process.
In this paper, the influence of frequency and temperature on the damping behaviour of bromobutyl rubber is presented. The material is modelled by a generalized Maxwell model, which can be implemented in finite element (FE) calculations for damping layout. Additionally, a novel setup for local CLD treatment is introduced, causing higher shear strain in the core layer. The damping results are compared to those of different damping treatments. Finally, the impact of bromobutyl rubber on the damping capability of the local CLD treatment is examined for various excitation frequencies and temperature levels.

Keywords: Viscoelasticity, Vibration Damping, Damping Layout
I-INCE Classification of Subject Number: 42, 47, 76

1. INTRODUCTION

In the construction of aeronautic structures, lightweight design is mandatory. Lightweight structures, as frames and stringers, are characterized by having high stiffness and low mass at the same time, as a consequence, they are prone to vibration. Especially an aircraft fuselage is composed of frames and stringers, visualized in Figure 1.
Vibrations introduced into the fuselage are transmitted as structure-borne sound. Structure-borne sound may radiate at fuselage skin and contribute to the cabin interior

[1]martin.groehlich@dlr.de
[2]marc.boeswald@dlr.de
[3]rene.winter@dlr.de

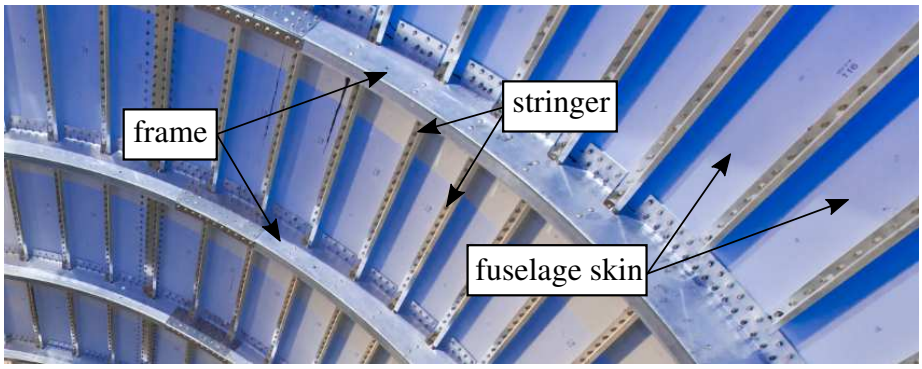

Figure 1: Fuselage composition of Flight-LAB-demonstrator

noise. The transmission of structure-borne noise at steady-state excitation, e.g. by turbulent boundary layer or engine induced vibration, can be reduced by increasing damping of the frames. For simplicity, these frames are initially considered as free-free supported straight beams. Damping increase can be achieved, by forcing an applied viscoelastic material into shear strain. A popular layout for vibration damping is the Constrained Layer Damping treatment (CLD), where a viscoelastic core layer is constrained between a stiffer base and face layer. Since a full coverage CLD treatment causes too much weight penalty, local damping patches shall be placed at proper positions of the beam and connected to each other, in order to increase shear strain. Considering a free-free vibrating beam, shown in Figure 2, points on the neutral fibre of the beam only perform vertical displacement, while points located on top or bottom surface also perform horizontal displacement due to the inclination of the neutral fibre. Using the fact, that the centre of the beam suffers only vertical displacement, a simple straight and in-plane cantilever beam model can be derived.

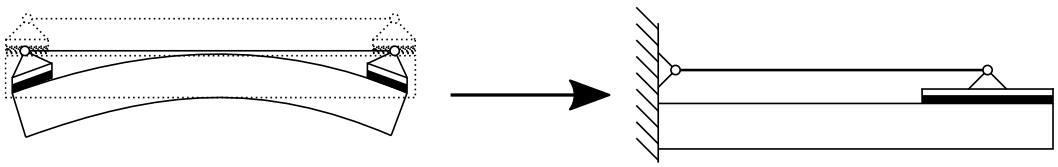

Figure 2: Idea of an improved local CLD treatment

Nevertheless, the essential component for damping layout is the viscoelastic material. Its damping properties change considerably under different conditions as excitation frequency and temperature. In order to design an appropriate damping layout of a structure, these influences need to be considered as well.
The main objective of this paper is to quantify the damping capabilities of the above-presented local CLD treatment with respect to frequency and temperature dependence. First, the theoretical background of frequency and temperature dependent viscoelastic material modelling as well as the integration in finite element (FE) analysis is demonstrated. Next, a simple parameter study is performed, pointing out the issues of the local CLD treatment. Afterwards, a comparison to other well established damping treatments is presented. Finally, a realistic viscoelastic material is introduced, showing the property changes and their impact on the damping capability of the local CLD treatment.

2. THEORETICAL BACKGROUND OF VISCOELASTIC MATERIAL MODELLING

In this section, the basics of idealized viscoelastic material modelling are exemplified. The essential properties are demonstrated and a formulation of the material behaviour in frequency domain is provided. Additionally, the temperature dependence on the material behaviour is implemented in the material model. By using the finite element method (FEM) it will be shown, how viscoelastic properties can be integrated to physically model local viscoelastic damping and to establish a global damping matrix for the structure.

2.1. Linear viscoelasticity in frequency domain

Under the assumption of a harmonic excitation, a viscoelastic material behaviour can be described in terms of a complex modulus, which is a function of the excitation frequency Ω. If constant temperature is assumed, the complex shear modulus G^* can be written as:

$$G^*(\Omega) = G'(\Omega) + i\,G''(\Omega) \tag{1}$$

The real part of the complex notation G' is the storage modulus and denotes the elastic behaviour of the material. In contrast to it, the imaginary part G'' is the loss modulus and denotes the viscous or dissipative properties. Both, the real and imaginary part can be expressed by using the parameters of a generalized Maxwell model, often referred to as Prony series. The composition and effects of a generalized Maxwell model are examined in [1] and [2]. The equation for the storage modulus leads to

$$G'(\Omega) = G_0\left[1 - \sum_{i=1}^{n}\left(\alpha_i - \frac{\alpha_i\,\tau_{rel,i}^2\,\Omega^2}{1 + \tau_{rel,i}^2\,\Omega^2}\right)\right], \tag{2}$$

where G_0 is the instantaneous shear modulus at infinitely high frequency, $\tau_{rel,i}$ the relaxation time and α_i the so called relative modulus [3]. The equation of the loss modulus is formulated as [3]:

$$G''(\Omega) = G_0\sum_{i=1}^{n}\left(\frac{\alpha_i\,\tau_{rel,i}\,\Omega}{1 + \tau_{rel,i}^2\,\Omega^2}\right) \tag{3}$$

The relation of both parts defines the loss factor η:

$$\eta(\Omega) = \frac{G''(\Omega)}{G'(\Omega)} \tag{4}$$

Concerning damping layout, the loss factor is the most important parameter as it quantifies the energy dissipation capability of a material. It is also known as the $tan\,\delta$ resulting from dynamic mechanical analysis (DMA).

2.2. Temperature dependence on viscoelastic material properties

The temperature dependence on material properties are taken into account by different shift factors. There are various approaches found in the literature regarding the shift factor calculation, e.g. in [4]. However, it should be taken into account, that the selection of the approach for the shift factor calculation highly depends on the given material and considered temperature region. In the scope of this paper, the Williams-Landel-Ferry

(WLF) as well as the Arrhenius approach are used and briefly presented in the following. For analysing the material properties' dependence of the temperature, two shifts have to be considered:

- Horizontal shift along the frequency axis due to thermal activated rearrangements and higher reaction rate on a molecular level
- Vertical shift along the material property axis due to changes in the type and amount of molecular processes

The frequency shift is defined by a horizontal shift factor ξ_H, resulting from the empirical WLF equation with experimentally determined constants $C1$ and $C2$ relating to a reference temperature T_0 [5]:

$$log\left(\xi_H(T,T_0)\right) = -\frac{C1\cdot(T-T_0)}{C2+T-T_0} \tag{5}$$

For the description of the vertical shift, the Arrhenius approach is used. The relation between the experimentally determined activation energy E_A concerning a temperature shift yields the vertical shift factor ξ_V [5]:

$$log\left(\xi_V(T,T_0)\right) = \frac{0,43\cdot E_A}{R}\left(\frac{1}{T}-\frac{1}{T_0}\right) \tag{6}$$

The parameter R is the universal gas constant. Considering a reference state $S_0(T_0, f_0, G'_0, G''_0, \eta_0)$, the corresponding shifted state $S_1(T_1, f_1, G'_1, G''_1, \eta_1)$ at an arbitrary temperature T_1 can be determined. If the vertical shift factors for storage and loss modulus are assumed to be unequal, the shift is calculated by Equations 7 and 8:

$$f_1 = f_0\cdot\xi_H \tag{7}$$

$$G'_1(f_1) = G'_0(f_0)\cdot\xi_{V,G'} \quad , \quad G''_1(f_1) = G''_0(f_0)\cdot\xi_{V,G''} \quad , \quad \eta_1 = \frac{G''_1}{G'_1} \tag{8}$$

A typical temperature shift of the storage modulus, loss modulus (a) and loss factor (b) of a virtual viscoelastic material, modelled with a generalized Maxwell model, is presented in Figure 3. It can be seen in both diagrams, that the characteristic course of all properties

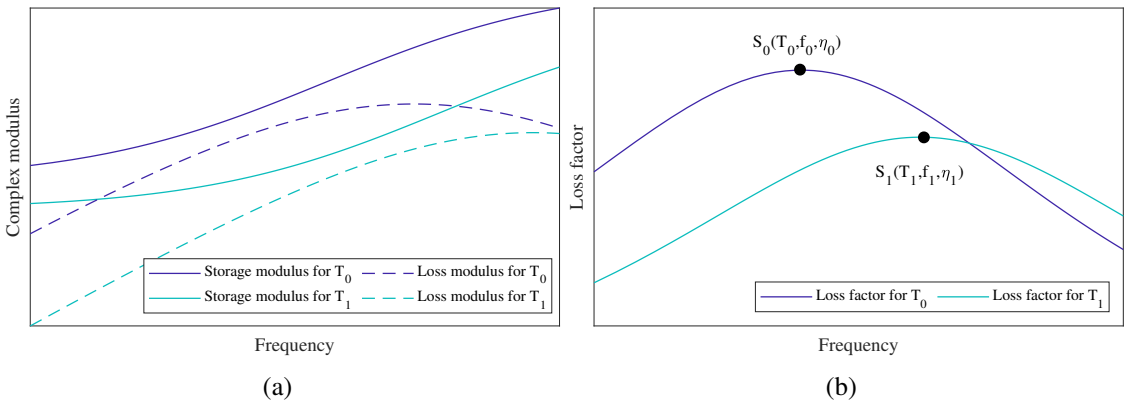

Figure 3: Complex modulus (a) and loss factor (b) during a temperature shift

stays the same, but shifted in horizontal and vertical direction. Especially Figure 3 (b) points out both shift directions clearly, since the maximum of the loss factor from the reference state S_0 decreases at a higher frequency for a different temperature (S_1).

2.3. Implementation of viscoelasticity into the finite element method

In order to integrate viscoelastic material properties into a spatial discretized continuum, a transformation from the one-dimensional material model into a three-dimensional is mandatory. Assuming isotropy as an additional material property, the transformation is carried out by Hooke's law. The relationship between stresses $\boldsymbol{\sigma}$ and strains $\boldsymbol{\epsilon}$ is determined by an elasticity matrix $\mathbf{E}$ [6]:

$$\boldsymbol{\sigma} = \mathbf{E} \cdot \boldsymbol{\epsilon} = \begin{bmatrix} \sigma_{xx} \\ \sigma_{yy} \\ \sigma_{zz} \\ \tau_{xy} \\ \tau_{xz} \\ \tau_{yz} \end{bmatrix} = \frac{E}{(1+\nu)(1-2\nu)} \begin{bmatrix} 1-\nu & \nu & \nu & 0 & 0 & 0 \\ \nu & 1-\nu & \nu & 0 & 0 & 0 \\ \nu & \nu & 1-\nu & 0 & 0 & 0 \\ 0 & 0 & 0 & \frac{1-2\nu}{2} & 0 & 0 \\ 0 & 0 & 0 & 0 & \frac{1-2\nu}{2} & 0 \\ 0 & 0 & 0 & 0 & 0 & \frac{1-2\nu}{2} \end{bmatrix} \cdot \begin{bmatrix} \epsilon_{xx} \\ \epsilon_{yy} \\ \epsilon_{zz} \\ \gamma_{xy} \\ \gamma_{xz} \\ \gamma_{yz} \end{bmatrix} \tag{9}$$

The stress and strain vectors include their corresponding spatial normal parts σ and ϵ, as well as the spatial shear parts τ and γ. Furthermore, the Young's modulus E and the shear modulus G are both related to the Poisson's ratio ν [6]:

$$E = 2G\,(1+\nu) \tag{10}$$

At this point it should be noted, that the elasticity matrix consists of complex entries, as far as viscoelasticity is applied. In this case, the elasticity matrix can be divided up into a real and imaginary part, representing storage and loss behaviour:

$$\mathbf{E}^*(\Omega, T) = \mathbf{E}'(\Omega, T) + i\,\mathbf{E}''(\Omega, T) \tag{11}$$

Based on the equivalence of virtual work of external loads with the virtual work of internal stress and strain, a complex stiffness matrix for a finite element can be assembled:

$$\mathbf{K}_E^*(\Omega, T) = \int_{V_E} \left(\boldsymbol{\Theta}\boldsymbol{\varphi}^T\right)^T \mathbf{E}^*(\Omega, T)\, \boldsymbol{\Theta}\boldsymbol{\varphi}^T dV_E \tag{12}$$

$\boldsymbol{\Theta}$ denotes the differential operator matrix, whereas $\boldsymbol{\varphi}$ conform to the matrix of shape functions. Considering the complex notation of Equation 11, Equation 12 yields a real element stiffness matrix as well as an hysteretic element damping matrix $\mathbf{D}_E$:

$$\mathbf{K}_E(\Omega, T) = \int_{V_E} \left(\boldsymbol{\Theta}\boldsymbol{\varphi}^T\right)^T \mathbf{E}'(\Omega, T)\, \boldsymbol{\Theta}\boldsymbol{\varphi}^T dV_E \tag{13}$$

$$i\,\mathbf{D}_E(\Omega, T) = i \int_{V_E} \left(\boldsymbol{\Theta}\boldsymbol{\varphi}^T\right)^T \mathbf{E}''(\Omega, T)\, \boldsymbol{\Theta}\boldsymbol{\varphi}^T dV_E = i\,\eta(\Omega, T)\,\mathbf{K}_E(\Omega, T) \tag{14}$$

Using the Boolean matrices $\mathbf{B}_E$, local viscoelastic elements are sorted into global stiffness and hysteretic damping matrices of the whole structure:

$$\mathbf{K}(\Omega, T) = \sum_E \mathbf{B}_E^T\, \mathbf{K}_E(\Omega, T)\, \mathbf{B}_E \tag{15}$$

$$i\,\mathbf{D}(\Omega, T) = i \sum_{E} \mathbf{B}_E^T\, \mathbf{D}_E(\Omega, T)\, \mathbf{B}_E \tag{16}$$

Due to this procedure, it is possible to integrate viscoelastic material as local dampers for example in composite structures.

3. CHARACTERISTICS OF LOCAL CLD TREATMENT

For the following analyses, the modal analysis application of commercial FE software ANSYS 17.2 is used. Two-dimensional structural solid elements called PLANE182 are chosen for element modelling as they have the feature to realise damping by a loss factor with respect to frequency and temperature dependence, which is needed in the later part [3]. However, under stationary condition, the material properties shall be considered as constant for comparability purpose. In the subsequent subsections, the modal loss factor η_k is used for damping estimation. Using the modal strain energy method [7], the modal loss factor is calculated as

$$\eta_k = \frac{\sum_{j=1}^{n} \eta_{j,k}\, U_{j,k}}{U_{total,k}}, \tag{17}$$

where $\eta_{j,k}$ is the loss factor and $U_{j,k}$ the modal strain energy of layer j at mode k, while $U_{total,k}$ denotes the total modal strain energy of the whole system at mode k. The modal loss factor can be converted into The conditions for a good loss factor estimation with the modal strain energy method are mentioned in [7] and considered as fulfilled.

3.1. Parameter study

The basic structure of the simulation is a simple aluminium cantilever beam with a rectangular cross section, as shown in Figure 4. By adding viscoelastic material with an aluminium face sheet in various configurations, the vibration of the beam is damped. The viscoelastic material is assumed to be in perfect contact with the beam and the face sheet.

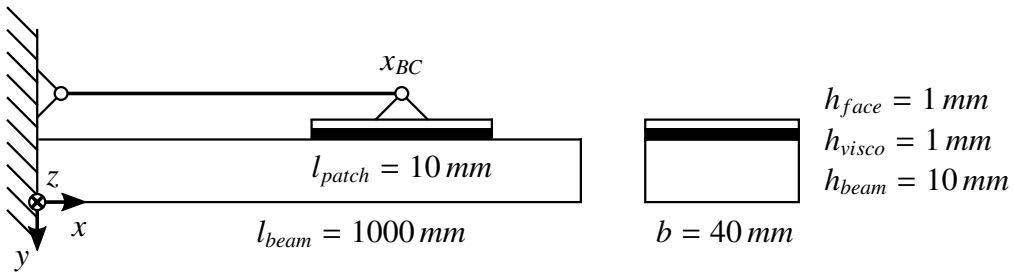

Figure 4: Geometrical setup of the local CLD treatment for the parameter study

The initial values for aluminium and the viscoelastic material are listed in Table 1. While frequency and temperature have an influence on material properties, the Youngs's modulus as well as the loss factor of the viscoelastic material differ during the parameter study in order to examine their effect on the damping capability separately.
Another parameter is the location of the damping patch, represented by the coordinate of the boundary condition x_{BC} at the centre of the patch. During the parameter study, the damping patch is placed at various positions from the fixed to the free end of the beam. The shown auxiliary mechanism is assumed to be massless and can be realised in the

Table 1: Initial properties of aluminium and a virtual viscoelastic material

	$\rho\,[\frac{kg}{m^3}]$	$E\,[Pa]$	$\nu\,[-]$	$\eta\,[-]$
Aluminium	2700	$7,1 \cdot 10^{10}$	0,33	0,005
Viscoelastic material	1000	$5 \cdot 10^{8}$	0,499	0,8

FE model by inserting the boundary condition in terms of a nodal constraint, blocking displacement in x-direction. The influence of the Young's modulus and the location of the boundary condition on the modal loss factor of the 4th mode are visualized in Figure 5. Mode 4 is chosen as a representative for the occurring effects. All these effects can be also detected for lower modes, but with a different intensity.

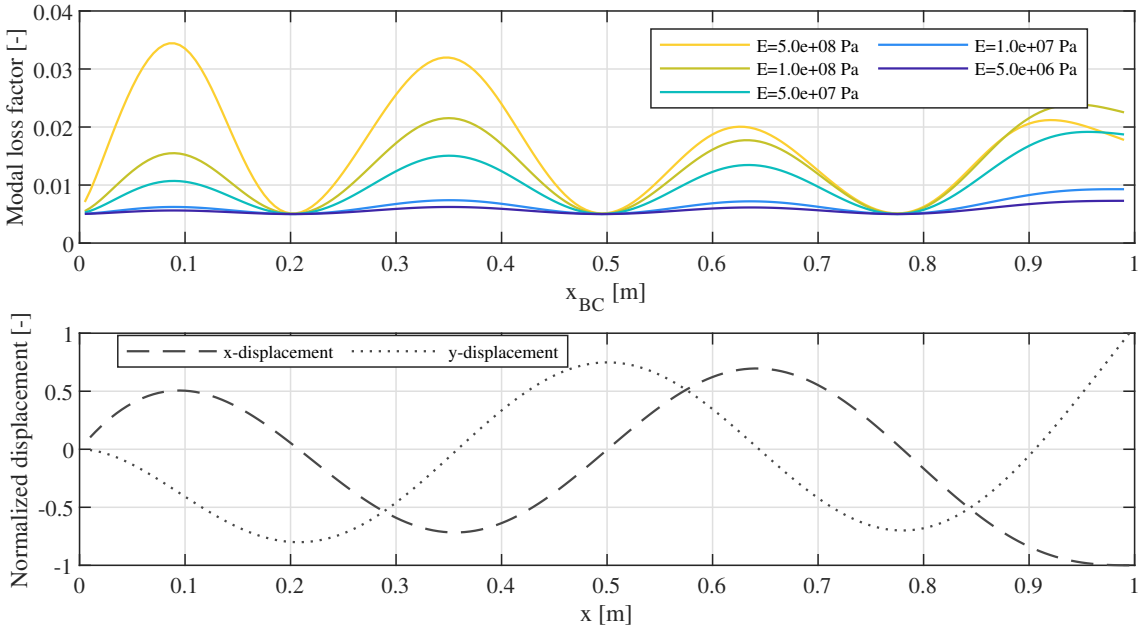

Figure 5: Modal loss factor of the damped beam (u.) due to stiffness variation and normalized displacements of the undamped beam at the surface (b.) for the 4th mode

It can be seen in the upper graph of Figure 5, that four local maxima occur. Regardless of the behaviour near the free end, ($x \geq 0,9\,m$), it is possible to notice that the stiffer the viscoelastic material, the higher the modal loss factor at its peaks. If the material is too soft, almost no increase of the modal loss factor is detected. Comparing the upper graph with the graph of the normalized x-displacement of the undamped beam, a correlation can be identified. Highest damping appears at locations with highest x-displacement, which are the vibration nodes of the y-displacement. Hence, a rule of thumb can be derived, that a damping patch has to be placed at such positions in order to obtain maximum damping values. This enables a targeted damping layout for selected modes of an arbitrary structure. The different behaviour at the free end may result from the increasing stiffness in combination with the boundary condition. If the stiffness is too high, shear deformation in the viscoelastic layer is hardly possible. In this case, the free end rather acts as another boundary condition and impacts the mode shape. If it is too low, the loss modulus will also become low and in consequence, no vibration energy is dissipated. From this point of view it can be derived, that an optimal stiffness exists for a damping patch positioning at the free end.

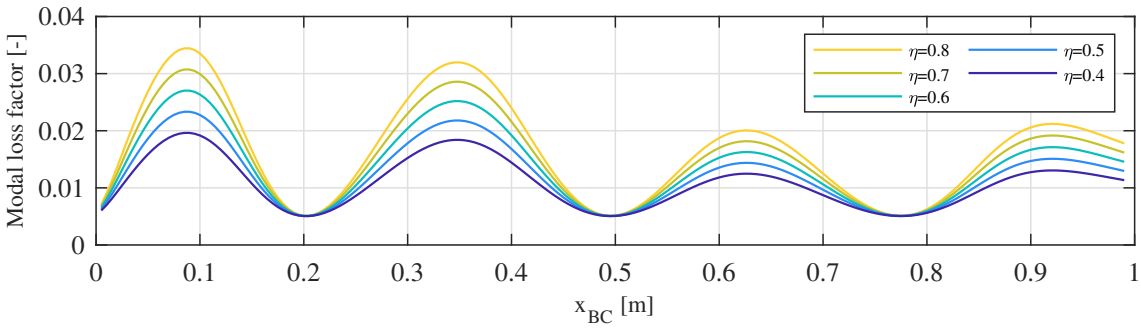

Figure 6: Modal loss factor due to loss factor variation for the 4th mode

A different behaviour can be observed for the loss factor variation, illustrated in Figure 6. The loss factor acts like a proportional factor. The higher it is, the higher is the resulting modal loss factor. Compared to the stiffness variation, the effect of the loss factor is not influenced by the location of the boundary condition.

3.2. Comparison to existing damping treatments

In order to demonstrate the effectiveness of the local CLD treatment, a comparison between different damping treatments is presented. For this purpose, the damping capability of full coverage Free Layer Damping (FLD) as well as full coverage CLD treatment is additionally evaluated. Each simulation is performed, applying the material properties from Table 1. For the FLD treatment, the thickness of the viscoelastic layer from Figure 4 is chosen to be $h_{visco} = 2\,mm$. In the case of CLD, the full beam is covered with a viscoelastic layer and a face sheet, but no auxiliary mechanism is applied. Therefore, the thickness of the viscoelastic layer and face sheet, shown in Figure 4, is used. The scope of the comparison includes the modal loss factor at the first four modes. The results are outlined in Figure 7. For local CLD treatment, the maximum achievable modal loss factor values are displayed, which result from the parameter variation of x_{BC}.

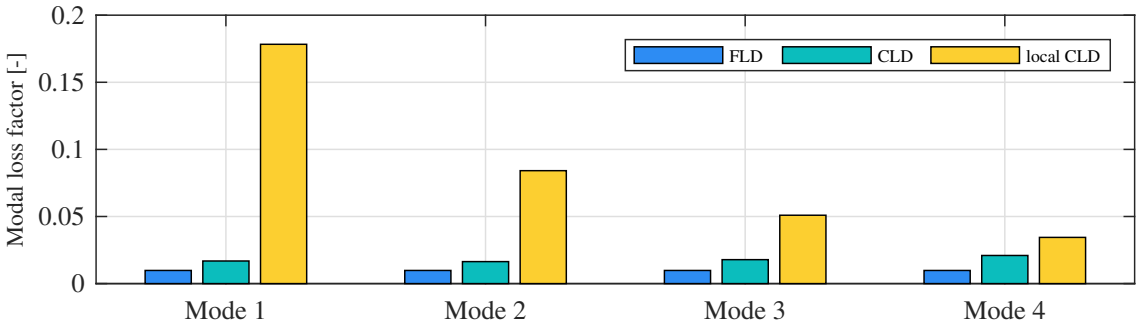

Figure 7: Modal loss factor of different damping treatments

From Figure 7 it becomes obvious, that the local CLD treatment has the best damping capability at all modes. Especially in the first mode the difference is significant. The estimated modal loss factor is about $\eta_1 = 0.18$, which corresponds to a modal viscous damping ratio of $D = 9\%$. However, the effectiveness in terms of the modal loss factor decreases with higher modes. A reason for this is the decreasing x-displacement of the beam at higher frequencies. As a result, less shear strain is generated in the viscoelastic layer and less vibration energy is dissipated.
Another advantage of the local CLD treatment is based on the damping increase relating

to the volume gain. With only 0.2% of volume gain it is possible to obtain superior damping values, while the damping capability with 20% volume gain for full coverage FLD and CLD treatments is rather poor. It has to be considered, that the presented local CLD treatment is massless and idealized though. A realistic auxiliary mechanism, as the one shown in Figure 4, would further increase the volume gain. The effectiveness can be increased by geometrical optimization of the damping patch otherwise.

4. CONSIDERATION OF FREQUENCY AND TEMPERATURE DEPENDENCE

After the damping capability of the local CLD treatment has been examined with constant material values, the effect of a realistic, frequency and temperature dependent viscoelastic material is presented in the following sections.

4.1. Material properties of bromobutyl rubber

In cooperation with the German Institute of Rubber Technology (Deutsches Institut für Kautschuktechnologie e.V.) a dedicated mixture of bromobutyl rubber for aeronautic applications as vibration damper has been developed. The frequency dependence is modelled by twelve parameter sets of the generalized Maxwell model, the temperature dependence by the presented WLF and Arrhenius approaches. In Figure 8, the essential material properties in terms of damping layout are illustrated.

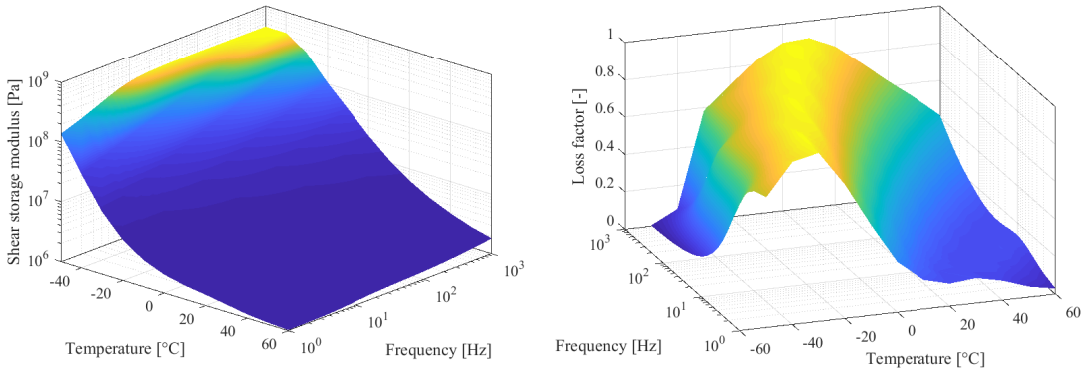

(a) (b)

Figure 8: Shear storage modulus (a) and loss factor (b) of bromobutyl rubber

For the shear storage modulus in Figure 8 (a), a considerable reduction can be detected, as temperature rises. Maximal stiffness of $G' = 4,5 \cdot 10^8\, Pa$ exists at lowest temperature of $T = -50\,°C$ and highest frequency of $f = 500\,Hz$. At a temperature of $T = 60\,°C$, the shear storage modulus is more than thousand times less than at $T = -50\,°C$.
A more complicated behaviour can be observed for the loss factor in Figure 8 (b). In the temperature range from $-40\,°C \leq T \leq 10\,°C$, a region of highest loss factor values occurs. Within that range, the maximal loss factor values are about $\eta = 0.9$. However, the loss factor drops significantly outside that region. Especially for high temperatures in combination with low frequencies, the loss factor is close to zero. The same behaviour appears at low temperature and high frequency. Considering the results from the parametric study, bromobutyl rubber is a proper damping material for temperature regions below zero in the mid-frequency range. These conditions appear especially in

cruise flights, as the outdoor temperature is far below $0\,°C$ and when the vibroacoustic performance of the fuselage up to $500\,Hz$ is under consideration. On the other hand, the usage of bromobutyl rubber should be avoided for high temperatures, since it provides poor damping capability.

4.2. Impact of bromobutyl rubber on local CLD treatment

As presented in the previous section, the viscoelastic material properties vary significantly with temperature and frequency and the resulting impact on the damping capability of the local CLD treatment needs to be examined. For the following analysis, the setup from Figure 4 is modified. This time, the length of the damping patch as well as the thickness of the aluminium face sheet is increased. In order to ensure comparability during the analysis, the damping patch cuts off with the free end, as demonstrated in Figure 9.

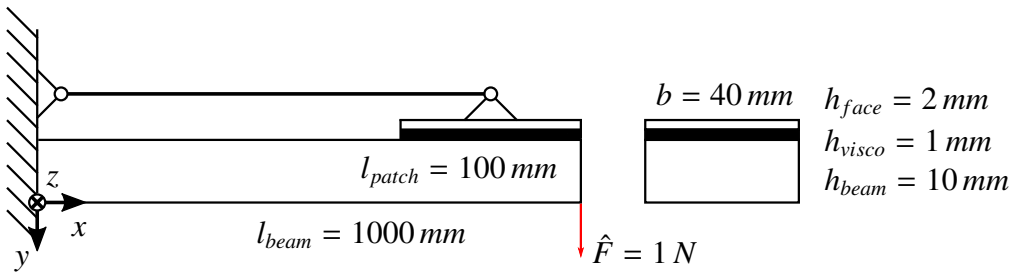

Figure 9: Modified geometrical setup of the local CLD treatment

Since is it not possible to include temperature and frequency dependence within a modal analysis study in ANSYS 17.2, a harmonic response analysis with a vertical force at the free end is performed. By using the peak-fit method [8], modal damping values of the first four identified eigenfrequencies are extracted from the recorded frequency response function. Thermal expansion of the components is neglected. The results are visualized in Figure 10. It should be noted, that the eigenfrequencies displayed at the x-axis are average values. Given the fact that stiffness changes due to temperature variations, eigenfrequencies also change. While the change is rather low for mode 1 and 2, the maximum difference within the fourth mode is approximately $20\,Hz$. Additionally, the damping due to structural damping of the aluminium is drawn with a dashed horizontal line. In Figure 10 it can be seen, that the impact of both temperature and frequency on the damping capability is substantial. Taking the first mode, the damping ratio can vary from no viscoelastic damping ($T = -50\,°C$) to $4,5\%$ damping ratio ($T = 0\,°C$). By

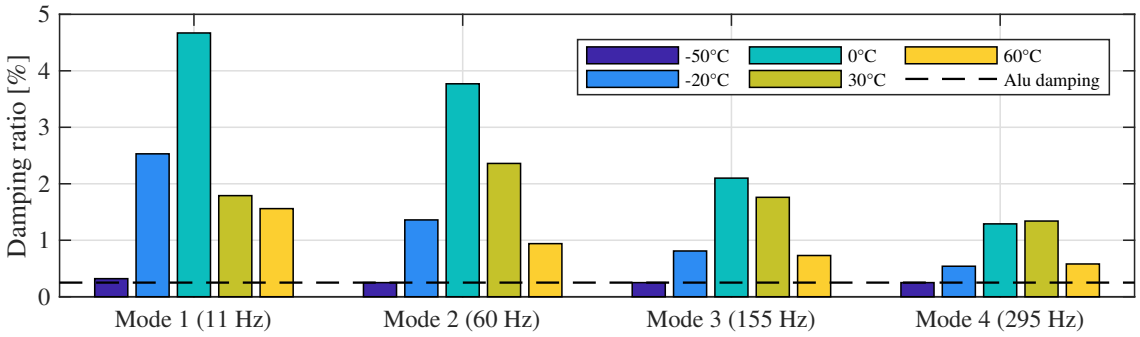

Figure 10: Influence of frequency and temperature on modal damping capabilities

considering each temperature, a decrease of the damping ratio is detectable with rising frequency, as the shear deformation in the viscoelastic layer decreases. An exception is temperature $T = 30\,°C$, where the damping ratio of mode 2 is higher than at mode 1. Also the order of highest damping ratios varies with frequency. While the second highest value occur at a temperature of $T = -20\,°C$ at mode 1, the corresponding damping ratio for mode 2 is just third highest. Only the damping ratio of both lowest as well as highest temperature stay in the same order.
In order to find an explanation for the observed phenomena, an examination of the viscoelastic material properties from top view, shown in Figure 11, is helpful. The horizontal lines indicate the particular eigenfrequencies, the vertical ones are isothermal lines.

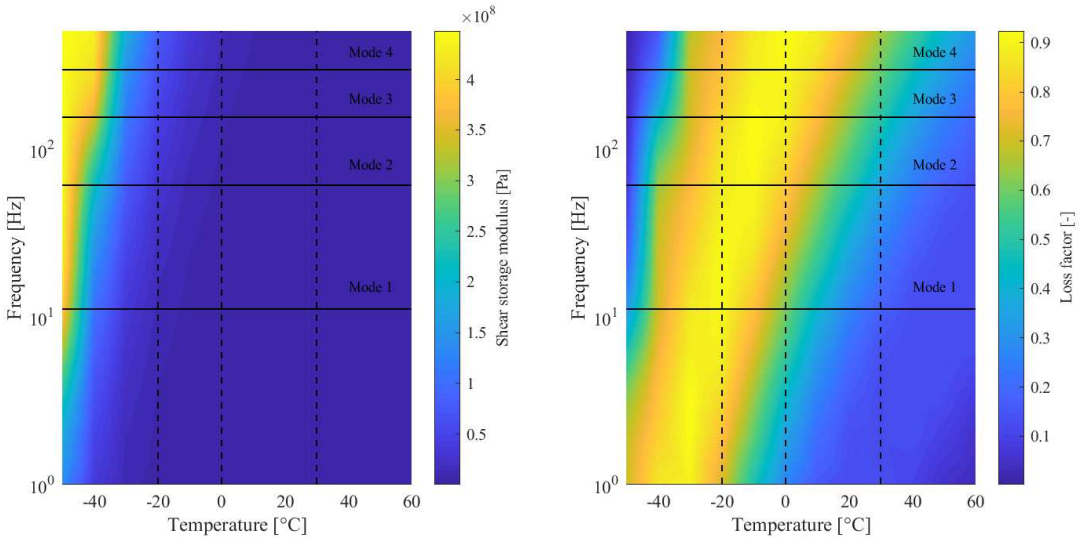

Figure 11: Top view on the contours of the shear storage modulus (a) and loss factor (b)

An explanation for smallest damping ratios at the lowest and highest temperature can be drawn from both images of Figure 11. While the storage modulus is maximal, the corresponding loss factor is minimal at the lowest temperature. As explained in section 3.1, the viscoelastic layer acts as another boundary condition and prevents movement. Concerning energy dissipation, both the stiffness and loss factor of the highest temperature is too low compared to those of the lowest temperature.
The importance of a proper storage modulus can be exemplified on basis of temperatures $T = -20\,°C$ and $T = 30\,°C$. Although the loss factor is explicitly higher for $T = -20\,°C$ in Figure 11 (b), the damping ratios for modes 2-4 are marginal compared to those of $T = 30\,°C$ in Figure 10. However, the storage moduli for $T = 30\,°C$ are much smaller than for $T = -20\,°C$, as apparent in Figure 11 (a). From that fact it can be drawn, that not only the loss factor, but also a proper storage modulus is decisive for high damping values.

5. CONCLUSIONS

In this paper, the modelling of viscoelastic material in frequency domain has been presented. Using the WLF and Arrhenius approaches, viscoelastic damping properties

are described additionally in terms of frequency and temperature dependent storage modulus and loss factor. The modelling is fully consistent and compatible with finite element modelling and allows for local damping modelling.
Furthermore, a novel concept of local CLD treatment has been introduced and analysed by a parameter study with virtual material properties. The influence of a damping patch position as well as the influence of storage modulus and loss factor on the modal loss factor have been examined. A rule of thumb has been derived, giving the designer advice, where to place a damping patch in a structure. The advantages of the local CLD treatment compared to full coverage FLD and CLD treatments have been outlined.
Finally, an application using a real existing viscoelastic material named bromobutyl has been presented and the impact on damping in terms of shear storage modulus and loss factor has been quantified. The significant property changes due to frequency and temperature variation have been illustrated and their influence on the local CLD treatment has been investigated. It was shown, that the damping capability varies considerably under different excitation frequencies and temperature levels. However, it was outlined, that not only a high loss factor is decisive for obtaining high damping values. Instead, an appropriate adjustment of both geometrical and material properties needs to be carried out.

6. REFERENCES

[1] W. Michaeli, M. Brandt, M. Brinkmann, and E. Schmachtenberg. Simulation des nicht-linear viskoelastischen werkstoffverhaltens von kunststoffen mit dem 3d-deformationsmodell. *Zeitschrift für Kunststofftechnik*, 2006.

[2] M. Böswald, M. Gröhlich, J. Biedermann, and R. Winter. Analysis and simulation of structures with local visco-elastic damping from elastomers. In *Proceedings of the International Conference on Noise and Vibration Engineering ISMA2018, Leuven, Belgium*, 2018.

[3] Ansys Inc. *Theory Reference for the Mechanical APDL and Mechanical Applications*. Ansys Inc., 2017.

[4] F. R. Schwarzl. *Polymermechanik: Struktur und mechanisches Verhalten von Polymeren*. Springer-Verlag, 1990.

[5] A. Scholz. *Ein Beitrag zur Optimierung des Schwingungsverhaltens komplexer Rotorsysteme mit viskoelastischen Dämpfungselementen*. PhD thesis, Technische Universität Berlin, 2011.

[6] M. Link. *Finite Elemente in der Statik und Dynamik*. Springer-Verlag, 2014.

[7] G. Lepoittevin and G. Kress. Optimization of segmented constrained layer damping with mathematical programming using strain energy analysis and modal data. *Materials & Design*, Vol. 31(No. 1):pp. 14–24, 2010.

[8] M. Böswald. Analysis of the bias in modal parameters obtained with frequency-domain rational fraction polynomial estimators. In *Proceedings of the International Conference on Noise and Vibration Engineering ISMA2016, Leuven, Belgium*, 2016.